Hydrodynamics of Fluidization in a Semicircular Bed with a Jet

A hydrodynamic model of fluidization was developed that computes void fractions, pressure and solid and gas velocities in cylindrical fluidized beds. Computed time-averaged gas velocity distributions of a jet compared well with Westinghouse experimental data without the use of any fitted parameters. The main empirical input was a drag correlation from the literature.

BOZORG ETTEHADIEH, DIMITRI GIDASPOW, and R. W. LYCZKOWSKI

Department of Chemical Engineering
Illinois Institute of Technology
Chicago, IL 60616

SCOPE

High rates of heat and mass transfer and solids mobility make the fluidized-bed reactors ideal for many solid-fluid reactions, such as gasification of coal. However, one of the largest concerns when using fluidized beds to commercialize many chemical processes is scale-up (Keairns, 1979). We believe this is due to the absence of an experimentally verified hydrodynamic theory that can describe the complicated transient gas and solid motion in a fluid bed.

During the past three years several organizations began to develop hydrodynamic computer models for a fluidized-bed gasifier that promise to be predictive in many respects (JAYCOR, S^3, IIT). In addition to providing a tool for scale-up and process optimization, these models help understand the chemical and physical behavior of the systems. These models are based on the early hydrodynamic theory of Jackson, (1963a,b, 1971). Jackson's equations reduce themselves to the popular Davidson's (1961) theory for the case of a constant void fraction (Lyczkowski et al., 1982). The S^3 and the IIT computer models calculate the pressure, the void fraction and the velocities of a single-size solid and of the gas. The fluid bed never reaches a steady state, but continually oscillates, as bubbles form, rise through the bed and erupt on top of the bed. Both models have the ability to compute a bubble size that compares well to experiments (S^3, Schneyer et al. 1981; Gidaspow et al., 1983a). The IIT model was found to be able to predict time averaged porosity distributions in a two-dimensional bed with a jet, (Gidaspow, 1981a,b). The input to the models must consist of independently measured correlations, such as the drag laws available in the literature and should ideally not involve parameters fitted from the experiment being modeled.

CONCLUSIONS AND SIGNIFICANCE

A numerically stable hydrodynamic computer model was developed for a cold fluidized bed that has only one empirical input; a drag relation from the fluidization literature. A solids' stress relation is used to remedy the inherent illposedness of Jackson's equations. This solids pressure or stress is generally very small numerically. The competitive S^3 model has other empirical input such as solids viscosities.

The results of the computer model agreed within the experimental error with the measured time averaged jet velocity profiles obtained at Westinghouse, Yang and Keairns (1980), in a semicircular bed with and without solid loading. No fitted parameters were used. There is also qualitative agreement with the results of solid velocity measured by Donsi et al. (1980).

The code can now be extended to model a real hot-bed gasifier by adding energy and conservation of species equations.

INTRODUCTION

To understand the dynamics of gas-solid motion in a fluidized-bed gasifier, a convenient device is a semicircular bed with a window to allow observation of the motion of bubbles. Such a device has been exploited with particular success by Yang and Keairns.

Yang and Keairns (1980) have published numerous data on local pressure and gas velocities in a semicircular fluidized bed. They measured the static and impact pressures at different locations in the bed by using U-tube and inclined manometers. The gas velocity is then found by setting the kinetic energy of the gas equal to the difference between the two pressures. Yang and Keairns (1981) have also reported data on solid entrainment velocities into the jetting region of the same semicircular bed by analyzing high-speed movies of the dyed particle movement in the bed.

Donsi et al. (1980) have measured axial solid and gas velocity profiles in cylindrical and semicircular beds for a variety of particles. They measured gas and solid velocities by using pitot tubes and high speed photography. They also utilized an impact probe to measure the number of particles crossing the jet cross-sectional area per unit time. They have thus been able to find the solid's volume fraction along the jet. They also attempted to analyse their experimental findings by using turbulent jet theory.

The K-FIX computer code (Rivard and Torrey, 1977) was modified and used to predict the flow behavior of cylindrical fluidized beds.

R. W. Lyczkowski is presently at the Argonne National Laboratory.

EQUATIONS OF MOTION

Hydrodynamic models of fluidization use the principles of conservation of mass, momentum and energy. The continuity and the separate phase momentum equations for transient two-phase flow in cylindrical coordinates are:

Gas Continuity

$$\frac{\partial \rho_g \epsilon}{\partial t} + \frac{1}{r}\frac{\partial \rho_s \epsilon U_g r}{\partial r} + \frac{\partial \rho_g \epsilon V_g}{\partial y} = 0 \tag{1}$$

Solid Continuity

$$\frac{\partial \rho_s (1-\epsilon)}{\partial t} + \frac{1}{r}\frac{\partial \rho_s (1-\epsilon) U_s r}{\partial r} + \frac{\partial \rho_s (1-\epsilon) V_s}{\partial y} = 0 \tag{2}$$

Gas Momentum Equation in r Direction

$$\frac{\partial \rho_g \epsilon U_g}{\partial t} + \frac{1}{r}\frac{\partial \rho_g \epsilon U_g^2}{\partial r} + \frac{\partial \rho_g \epsilon U_g V_g}{\partial y} = -\epsilon \frac{\partial P}{\partial r} + \beta_r (U_g - U_s) \tag{3}$$

Solid Momentum Equation in r Direction

$$\frac{\partial [\rho_s (1-\epsilon) U_s]}{\partial t} + \frac{1}{r}\frac{\partial [\rho_s (1-\epsilon) U_s^2 r]}{\partial r} + \frac{\partial [\rho_s (1-\epsilon) U_s V_s]}{\partial y} = -(1-\epsilon)\frac{\partial P}{\partial r} + \beta_r (U_s - U_g) - \frac{\partial \tau_{rr}}{\partial r} \tag{4}$$

where

$$\frac{\partial \tau_{rr}}{\partial r} = G(\epsilon)\frac{\partial \epsilon}{\partial r}, \tag{5}$$

Gas Momentum Equation in y Direction

$$\frac{\partial \rho_g \epsilon V_g}{\partial t} + \frac{1}{r}\frac{\partial \rho_g \epsilon U_g V_g r}{\partial r} + \frac{\partial \rho_g \epsilon V_g^2}{\partial y} = -\epsilon \frac{\partial p}{\partial y} + \beta_y (V_g - V_s) - \rho_g \epsilon g \tag{6}$$

Solid Momentum Equation in y Direction

$$\frac{\partial [\rho_s (1-\epsilon) V_s]}{\partial t} + \frac{1}{r}\frac{\partial [\rho_s (1-\epsilon) V_s U_s r]}{\partial r} + \frac{\partial [\rho_s (1-\epsilon) V_s^2]}{\partial y} = -(1-\epsilon)\frac{\partial p}{\partial y} + \beta_y (V_s - V_g) - \frac{\partial \tau_{yy}}{\partial y} - \rho_s (1-\epsilon) g \tag{7}$$

where

$$\frac{\partial \tau_{yy}}{\partial y} = G(\epsilon)\frac{\partial \epsilon}{\partial y} \tag{8}$$

In the equations of motion β_r and β_y are the friction coefficients between the gas and the solid particles.

According to Wen and Yu (1966) for porosities less than 0.8 the pressure drop due to friction between gas and solids can be described by the Ergun equation. Thus the friction coefficient in this porosity range becomes,

$$\beta_y = 150\frac{(1-\epsilon)^2 \mu_g}{\epsilon (d_p \phi_s)^2} + 1.75\frac{\rho_g |V_g - V_s| (1-\epsilon)}{\phi_s d_p}. \tag{9}$$

Rietma and Mutsers (1973) have also found a similar expression for β whose reciprocal they call mobility.

Wen and Yu (1966) have extended the works of Richardson and Zaki (1954) to derive an expression for pressure drop prediction in particulate beds. For porosities greater than 0.8 such a relation for pressure drop leads to the following expression for the friction coefficient.

$$\beta_y = \frac{3}{4} C_{dy}\frac{\epsilon (1-\epsilon) |V_g - V_s| \rho_g}{d_p \phi_s} f(\epsilon) \quad \epsilon \geq 0.8 \tag{10}$$

where C_{Dy}, the drag coefficient in y direction, is related to Reynolds number, Rowe (1961)

$$C_{Dy} = \frac{24}{Re_{sy}}(1 + 0.15 Re_{sy}^{0.687}) \quad Re_{sy} < 1{,}000 \tag{11}$$

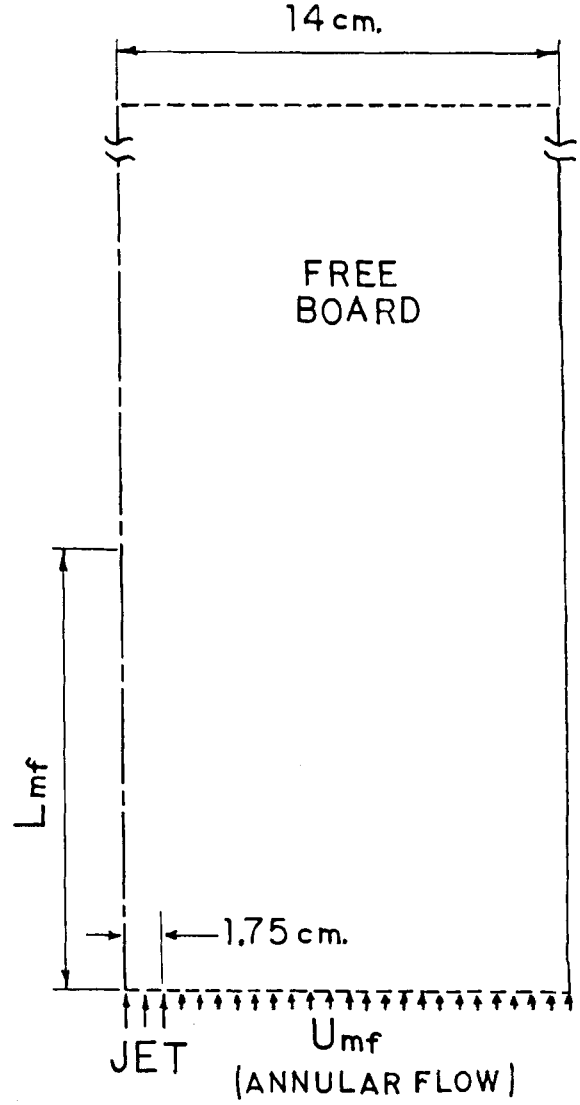

Figure 1. Geometry of the bed used in the numerical calculations.

$$C_{Dy} = 0.44 \qquad Re_{sy} \geq 1{,}000 \tag{12}$$

where

$$Re_{sy} = \frac{\epsilon \rho_g (V_g - V_s) d_p}{\mu_g} \tag{13}$$

In Eq. 10 $f(\epsilon)$ shows the effect due to the presence of other particles in the fluid and acts as a correction to the usual Stokes law for free fall of a single particle. We use

$$f(\epsilon) = \epsilon^{-2.65} \tag{14}$$

The expression for the friction coefficient in the radial direction is the same as that in the axial direction.

The terms τ_{rr} and τ_{yy} are the normal components of the solid phase stress tensor. In the absence of such terms the local values of the void fraction in the fluid bed become unrealistically low. Rietma and Mutsers (1973) have included such a term in their solid equation of motion. Kos (1977) has made measurements of such a term for sedimentation. He found it to be small compared to the hydrostatic pressure. The constitutive equation for the normal component of stress is

$$\tau = \tau(\epsilon) \tag{15}$$

Using the chain rule, in the y direction we obtain

$$\frac{\partial \tau}{\partial y} = \frac{\partial \tau}{\partial \epsilon}\frac{\partial \epsilon}{\partial y} \tag{16}$$

TABLE 1. PHYSICAL PROPERTIES OF THE GAS (AIR) AND SOLID PARTICLES (POLYETHELENE) (WESTINGHOUSE BED)

	Experiment	Computer Run
$\bar{d}_p$	0.28 cm	Same
ρ_s, kg/m^3	901	Same
U_{mf}, m/s	0.762 m/s	Same
ϵ_{mf}	Not Reported	0.407
T_g, T_s	293 K	Same

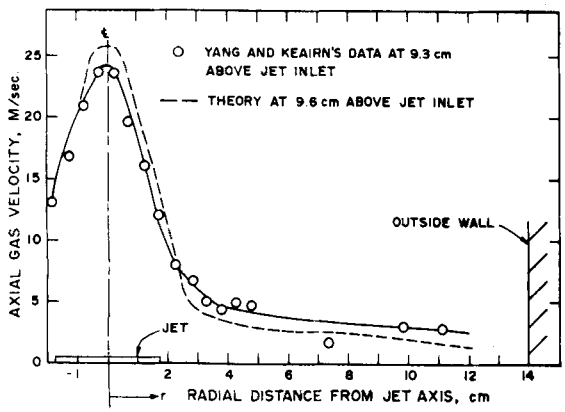

Figure 2. Experimental and time averaged theoretical axial gas velocities without solid loading in the jet at around 9.5 cm above gas inlet, V_{gjet} = 34.5 m/sec.

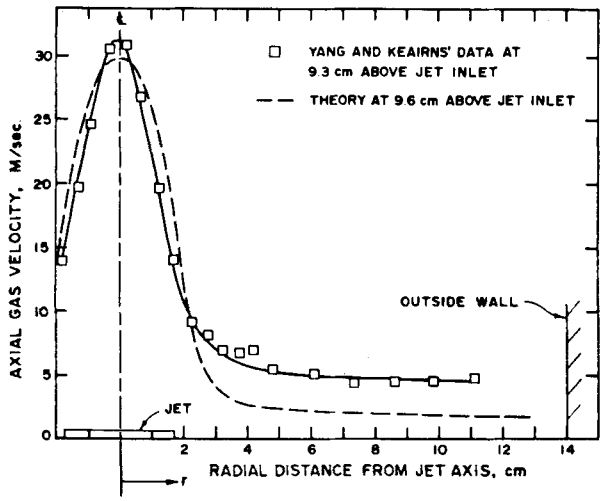

Figure 3. Experimental and time averaged theoretical axial gas velocities with solid loading in the jet at around 9 cm above gas inlet, V_{gjet} = 34.5 m/sec.

Pritchett et al. (1978) use the nomenclature, $G(\epsilon)$ for the modulus of elasticity or the particle-particle interaction coefficient, $\partial\tau/\partial\epsilon$, i.e.,

$$G(\epsilon) = \frac{\partial \tau}{\partial \epsilon} \tag{17}$$

An interpolation of Rietma and Mutser's data (1973) on glass beads and polypropylene particles was used for $G(\epsilon)$ in this study.

$$-G(\epsilon) = 10^{(-10.46\epsilon + 6.577)}, \text{ N/m}^2 \tag{18}$$

Numerical significance of this term is at porosities close to ϵ_{mf}. This term also improves the numerical stability of the system of equations by converting imaginary characteristics into real values. One of the characteristic directions, derived by Fanucci et al. (1979), for one dimensional incompressible flow for the set of conservation equations shown before is,

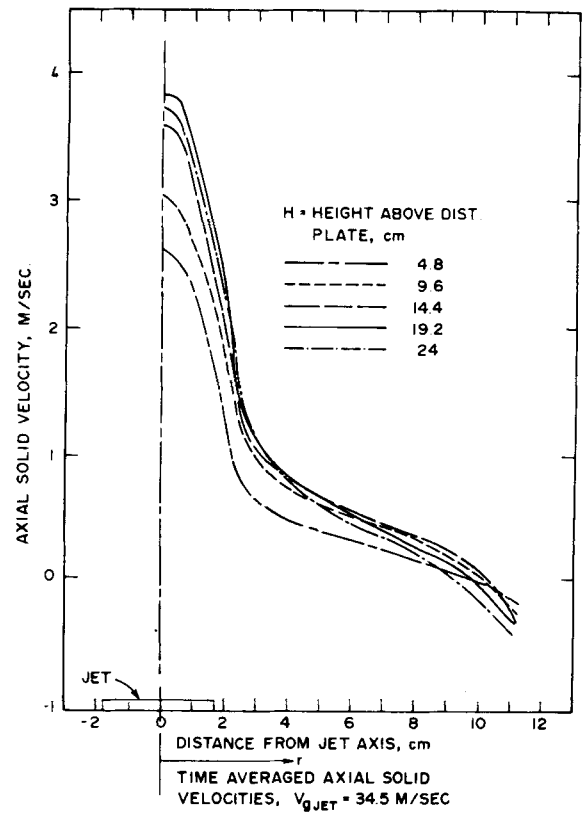

Figure 4. Time averaged axial solid velocities without solid loading in the jet, V_{gjet} = 34.5 m/sec.

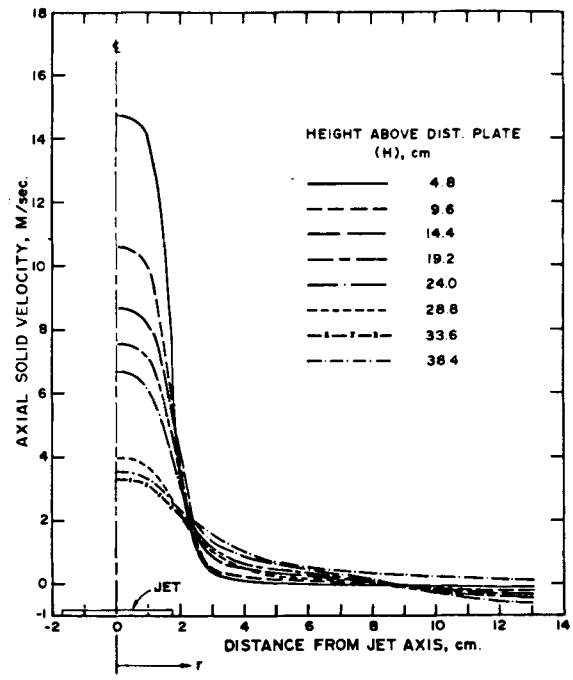

Figure 5. Time averaged theoretical axial solid velocities with solid loading in the jet, V_{gjet} = 34.5 m/sec.

$$C = \left[\frac{1}{\rho_{g/\epsilon} + \rho_{s/\epsilon_s}}\right]^{1/2}\left[\frac{-(V_g - V_s)^2}{\epsilon/\sigma_g + \epsilon_{s/\rho_s}} - \frac{G(\epsilon)}{\epsilon_s}\right]^{1/2} \tag{19}$$

In Eq. 19, as the value of porosity becomes smaller, $-G(\epsilon)$ becomes larger. This at porosities close to or below minimum fluidization, makes the characteristic, Eq. 19, real. The numerical results were found not to be greatly influenced when sensitivity runs were made

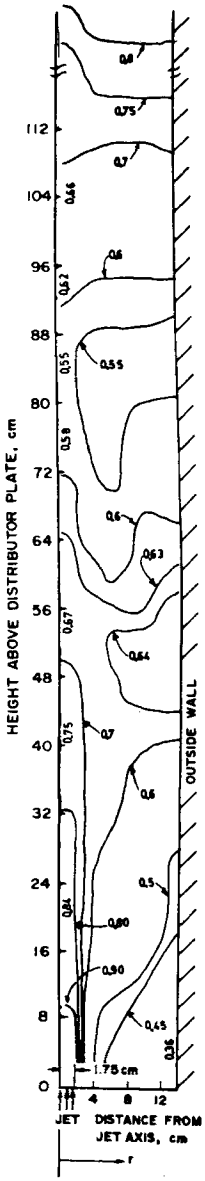

Figure 6. Time averaged porosity profiles without solid loading in the jet. $-G(\epsilon)=10^{(-10.46\epsilon+6.577)}N/M^2$.

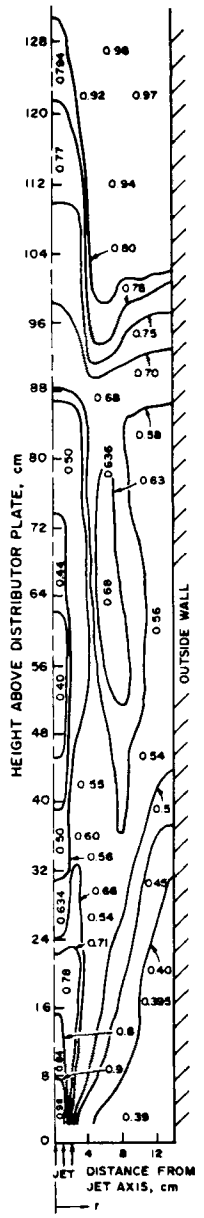

Figure 7. Time averaged porosity profiles with solid loading in the jet. $-G(\epsilon)=10^{(-10.46\epsilon+8.577)}N/M^2$.

for different values of $G(\epsilon)$ in two-dimensional beds (Ettehadieh, 1982).

NUMERICAL SOLUTION

The set of nonlinear partial differential equations was solved for U_s, U_g, V_s, ϵ and P using the numerics of the K-FIX program (Rivard and Torrey, 1977; Ettehadieh, 1982). The K-FIX code employs a staggered finite difference mesh system. Phase velocities are centered on cell boundaries, whereas all other quantities are centered at the center of the mesh. Mass and momentum fluxes across the cell boundaries are full donor cell differenced. The finite differenced equations were solved semiimplicitly, by a combination of point relaxation, Newton's and secant methods.

Instability problems were avoided by using the stabilizing solid stress term and large mesh sizes, as analyzed by Lyczkowski et al. (1978). Typical mesh sizes used in modeling of the Yang and Keairns experiment are Δr = 1.75 cm and Δz = 4.8 cm. The Courant stability condition of $\Delta t \leq \Delta z/V_{max}$ provides a relation for proper assignment of mesh sizes and time increment.

S^3 (Schneyer et al., 1981) and JAYCOR (Scharff et al., 1982) have also based their computation method on the ICE technique (Harlow and Amsden (1971), as described above.

COMPARISON OF THEORETICAL RESULTS TO WESTINGHOUSE DATA

The model bed used in the numerical computations is somewhat different from the actual fluid bed used by Yang and Keairns (1980). The grid flow section is eliminated and jet entrance is at level with the distributor plate through which minimum fluidizing gas flows. The jet entrance is also semicircular with its center at the center of the cylinder base. The geometry of the computational bed is shown in Figure 1. Data corresponding to runs GSF-44 and GSF-47 of Yang and Keairns were chosen for the computations. In both runs the jet gas velocity was 34.5 m/s. In run GSF-44 there is no solid loading in the jet flow, in run GSF-47 the solid loading is 2.75 wt. of solid/wt. of gas.

Physical properties of the gas and solid particles are shown in Table 1. The bed was assumed to be initially at minimum fluidization. The minimum fluidization porosity, ϵ_{mf}, was found by setting the bed weight equal to the pressure drop across the bed as

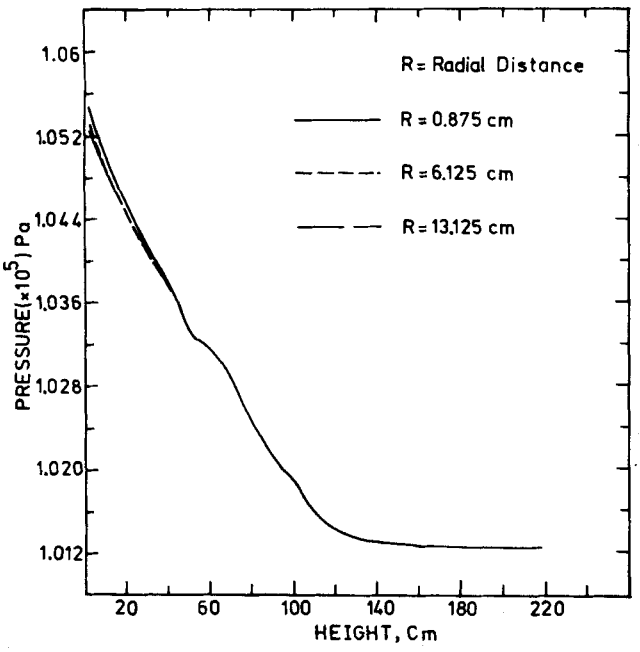

Figure 8. Time averaged pressure profiles across the cylindrical bed without solid loading in the jet, V_{gjet} = 34.5 m/sec.

given by the Ergun equation and solving iteratively for ϵ_{mf}.

Computed and time averaged, axial gas velocities are compared to the experimental results of Westinghouse in Figures 2 and 3. Figure 2 shows a close agreement between the theory and the experiment at around 9.6 cm. above jet inlet. It is also evident that the axial gas velocity is high close to the jet axis, and that it decreases very sharply and then flattens away from jet axis.

Experimental axial gas velocities with solid loading are on the average 5 to 8 m/s higher than those without solid loading. The difference between experimental and theoretical axial gas velocities is higher with solid loading than with no solid loading. Figure 3 shows a difference of 3 to 4 m/s between theoretical and experimental velocities. In the original Westinghouse bed, the gas flow rate through the grid region, which was about 30 cm above the distributor plate, was 1.99 m^3/min, compared to jet gas flow rate of 0.99 m^3/min. The comparison of the experimental and the theoretical axial gas velocities shows that the effect of grid flow elimination is more pronounced at higher heights and away from jet axis.

Time averaged theoretical axial solid velocities are shown in Figures 4 and 5. In the case of zero solid loading in the jet flow, Figure 4, the solid particle velocity increases along the jet axis, reaches a maximum velocity of 3.83 m/s at a height of 19.2 cm and then starts to decrease. With solid loading in the jet, the solid particles have to be conveyed by the gas in the jet before they enter the fluidized bed; the solid-gas slip velocity at the jet inlet has to be close to the particle terminal velocity at the jet loading conditions. Hence, the solid velocity is at its' maximum at the jet inlet, V_s = 26.575 m/s, and decreases along the jet axis, Figure 5.

Figure 6 shows the time-averaged computed porosity profiles for the jet without solid loading. Some of the solid particles are blown into the free board initially provided above the static bed height due to high jet gas velocity. The porosity remains at/or around its minimum fluidization value up to a height of 29 cm and away from the jet inlet. Figure 7 shows the porosity profiles with solid loading in the jet. In both Figures 6 and 7 there is a minimum in porosity along the jet axis. In Figure 6, the minimum in porosity is 80 cm above the jet axis. With solid loading in the jet, the minimum porosity moves to about 62 cm above the jet inlet. This may be due to the solid content of the entering jet.

In studying the experimental porosity distributions in two-dimensional rectangular beds, Gidaspow et al. (1983a) have defined the minimum height where the porosity of a location at the jet axis is equal to that at its vicinity as the jet penetration depth and compared this depth to literature correlations. This height is about 55 cm above jet inlet, Figure 6. This value compares to a jet penetration height of 67.2 cm found from the correlation given by Basov et al. (1969). The Yang and Keairns' (1981) correlation shows a penetration height of 56 cm. With solid loading in the jet, the minimum porosity moves to about 62 cm above the jet inlet. With solid loading in the jet the location on jet axis where porosity is close to the porosity of adjacent cells moves to about 80 cm above the jet inlet. The Yang and Keairns' correlation when modified for the additional momentum input into the bed due to jet solid content, gives a penetration height of 68 cm.

In Figure 8, time-averaged axial pressure profiles are shown at three different radial distances. These profiles show an almost linear pressure drop and that the axial pressure drop variation is minimal at different radial locations. The static bed height used in these computations was 86.4 cm. Thus the initial weight of the bed or the pressure drop at minimum fluidization is

$$\Delta p = \rho_s(1 - \epsilon_{mf})H_{mf}g \tag{21}$$

or

$$\Delta p = 4{,}527 \text{ Pa}$$

From Figure 8, the overall time averaged pressure drop at r = 0.875 cm is 4,320 Pa compared to 4,527 Pa at minimum fluidization. The difference between the two pressure drops can in part be attributed to the additional solids pressure term in the solids momentum equation.

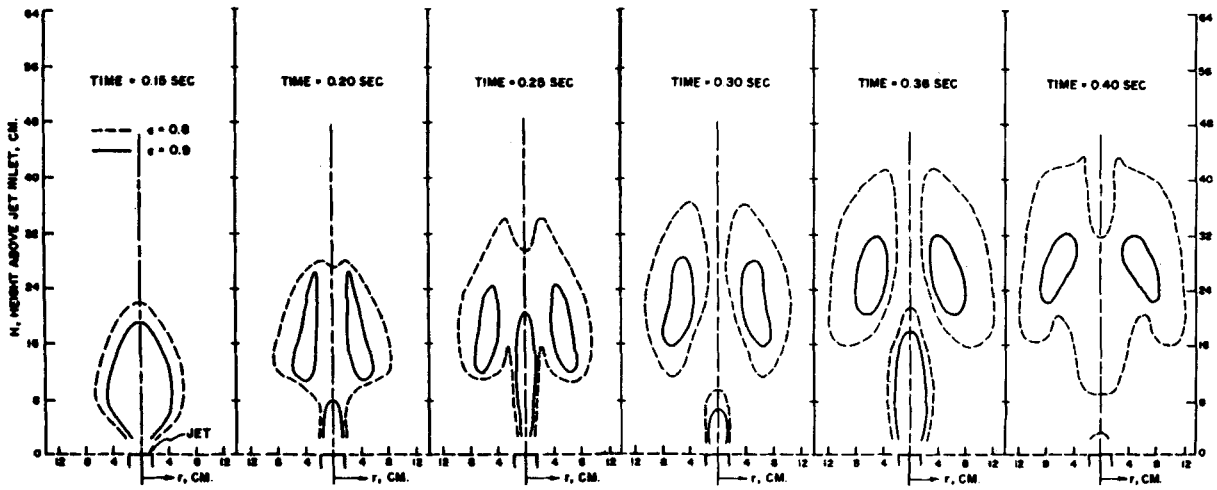

Figure 9. Growth and propagation of a void in a cylindrical bed with solid loading in the jet.

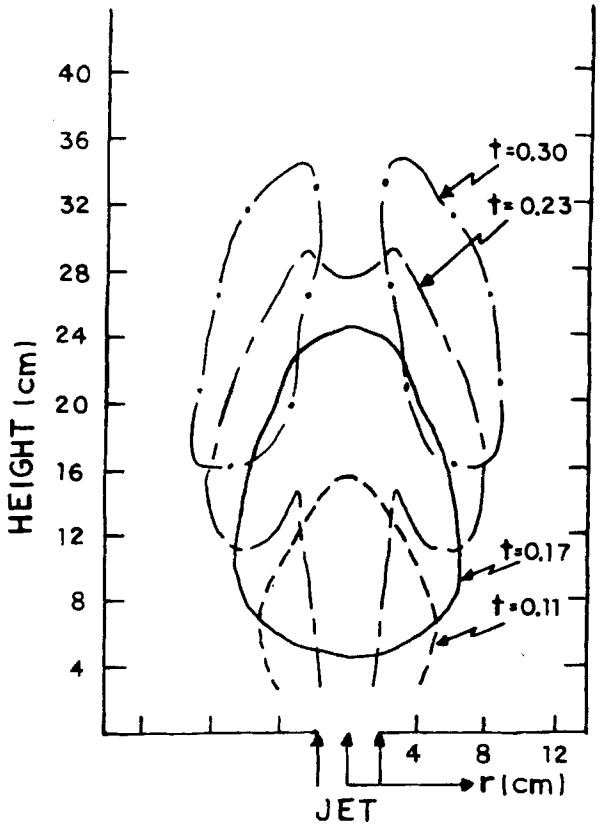

Figure 10. Formation of a toroidal bubble in a fluid bed with a jet.

TABLE 2. PHYSICAL PROPERTIES OF THE GAS (AIR) AND SOLID PARTICLES (PLASTIC BEADS) (DONSI ET AL.'S BED)

	Experiment	Computer Run
$\bar{d}_p$	0.29 cm	Same
ρ_s, kg/m^3	1,200	Same
U_{mf}, m/s	0.89	Same
H_{mf}, m	0.1	Same
ϵ_{mf}	Not Reported	0.397
V_{gjet}, m/s	90	Same
T_g, T_s, K	Not Reported	300

Figure 9 shows growth and movement of a void in the fluid bed, with solids entering via the jet gas flow. After the jet is turned on at time zero it forms a flame like jetting region above the inlet. A void or bubble is thus formed which disengages from the inlet as it rises in the bed. During the 0.2 to 0.3 s period the next flame-like region formed penetrates the first bubble and thus raises its solid content giving it a toroidal shape. This phenomenon was observed as bubbles splitting in two-dimensional beds (Gidaspow, et al., 1983b). During the 0.3 to 0.4 s period the next jetting region coalesces with the first bubble. As can be seen in Figure 9, the odd-shaped bubble or void at time 0.4 has a significant solid content which releases into the free board of the fluid bed subsequent to its eruption at the bed surface.

The contours of 0.8 porosities in the fluid bed with no solid loading in the jet gas flow are shown in Figure 10. At the 0.17 s instant in bed operation the region of 0.8 porosity and larger has just disengaged from the gas inlet. The diameter of a sphere of the same volume as this void is 14.3 cm. Davidson and Harrison's (1963) relation yields a diameter of 20.5 cm for a bubble formed at the gas inlet. In view of the simplifying assumptions in the Davidson and Harrison's approximate analytical formula, the comparison of the bubble sizes is good. There is a need to compare the theoretically calculated bubble sizes to photographs of bubbles. However, such data are not as yet available to the authors.

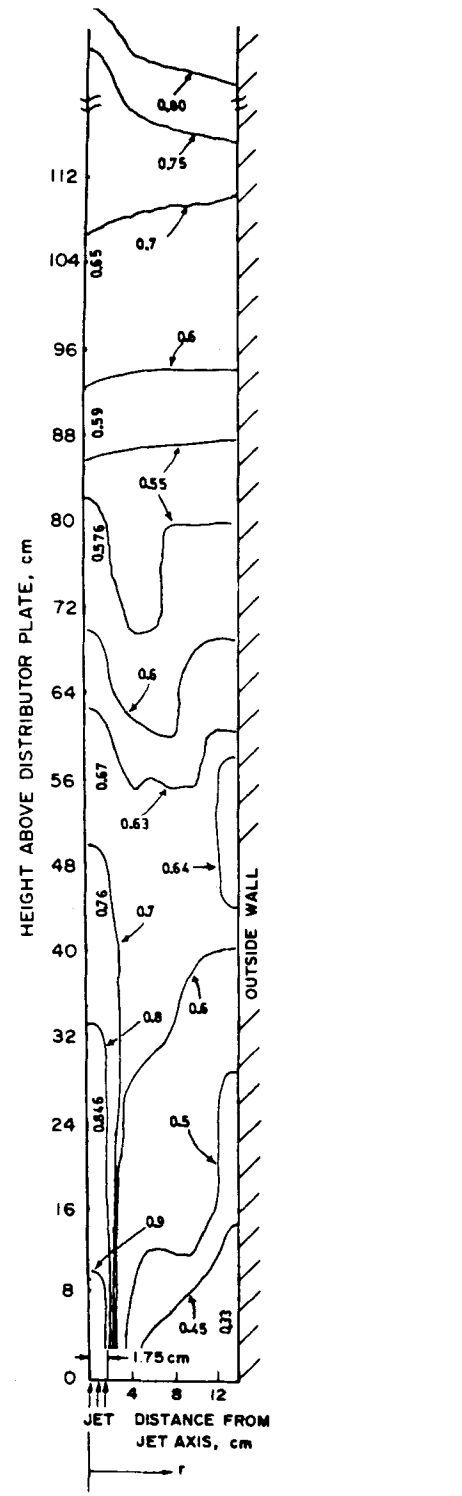

Figure 11. Time averaged porosity profiles without solid loading in the jet. $-G(\epsilon)=10^{(-8.76\epsilon+5.434)}N/M^2$.

SENSITIVITY TO THE SOLIDS PRESSURE

The solids pressure modulus, $G(\epsilon)$, plays two roles in the solution of the equations. It helps numerical stability and it prevents the particle volume fraction from becoming excessively high. Due to the unavailability of experimental data for $G(\epsilon)$ for the polyethylene particles, two extreme values of $G(\epsilon)$ from Rietma and Mutsers (1973) data for glass beads and polypropylene particles of size range 0–160 mesh were used. They are

$$-G(\epsilon) = 10^{(-8.76\epsilon + 5.43)}\text{N/m}^2 \qquad (22)$$

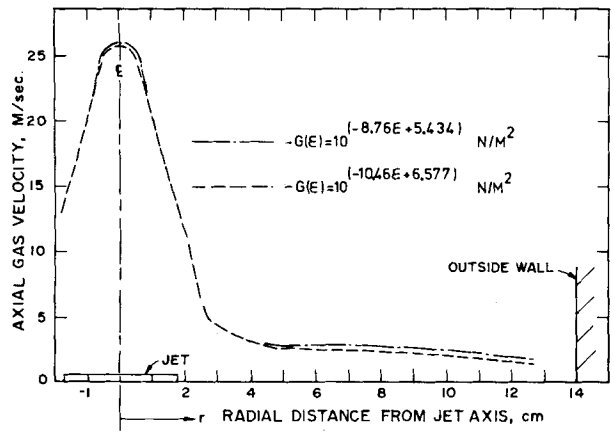

Figure 12. Effect of solids pressure modulus on time averaged velocities.

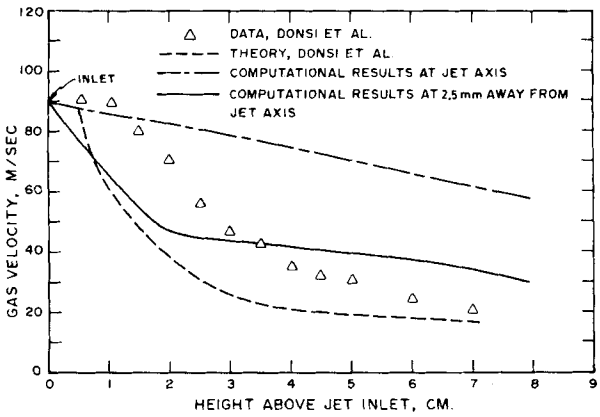

Figure 13. Experimental and time averaged theoretical axial gas velocities along the jet axis, V_{gjet} = 90 m/sec.

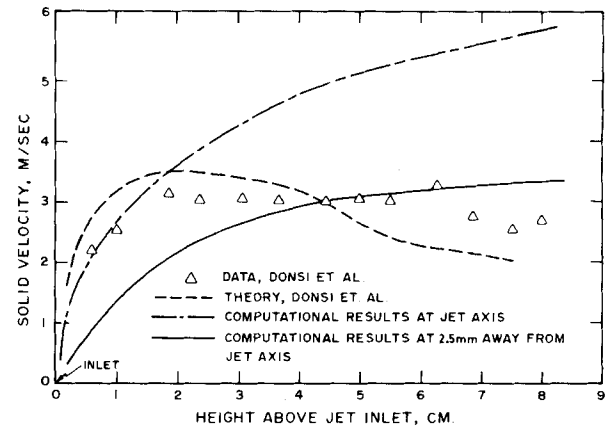

Figure 14. Experimental and time averaged theoretical axial solid velocities along the jet axis, V_{gjet} = 90 m/sec.

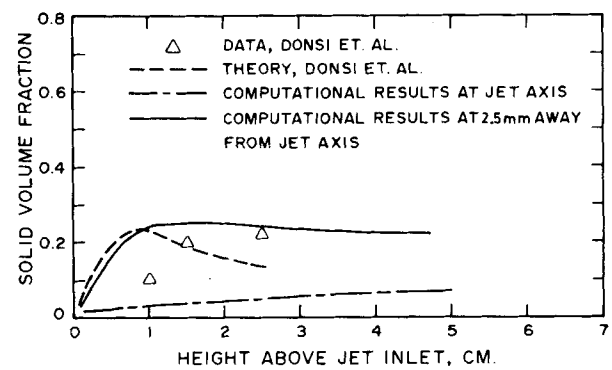

Figure 15. Experimental and time averaged theoretical solid volume fraction along the jet axis, V_{gjet} = 90 m/sec.

and $G(\epsilon)$ given by Eq. 18. At a minimum fluidization of 0.407, Eq. 18 yields a value of $G(\epsilon)$ of 209 N/m^2. Equation 22 gives 73 N/m^2.

Figure 11 shows the time-averaged porosity distribution with the new $G(\epsilon)$ calculated from Eq. 22. As can be seen from Figures 14 and 6 the major difference in the porosity distribution is at regions of porosity less than ϵ_{mf}, such as adjacent to the outside wall above the distributor plate. With $G(\epsilon)$ from Eq. 22 the areas close to the wall are more packed and the local porosities have fallen to below that of round spheres at packed-bed conditions. In Figure 12 the time-averaged axial gas velocities for the two different $G(\epsilon)$ are compared to each other at 9.6 cm above the jet inlet. The gas velocities are almost identical. The computed solids velocities were also very close to each other. Hence the numerical results are insensitive to the values of solids pressure moduli above minimum fluidization.

COMPARISON OF THEORETICAL RESULTS TO DONSI ET AL.'S EXPERIMENTAL DATA

Donsi et al. (1980) have measured the gas velocity by indirect measurement of pressure inside the jetting region. They have also measured the solid velocities by analyzing high-speed movies of the fluid bed. Impact probes were used to count the particles moving inside the jet and hence with estimates of solid velocities from the movies the void fraction inside the jetting region was found.

The experimental fluid bed was a cylinder, 16 cm in diameter with a 1 cm jet opening flush to the distributor plate at the center of the cylinder base. Initially the bed was assumed to be minimally fluidized at atmospheric pressure. Gas-solid properties and other related information are shown in Table 2. Minimum fluidization porosity was found as in Yang and Keairns fluid bed.

Profiles of axial gas velocities presented by Yang and Keairns (1980), also measured by pitot tubes, show the gas velocity to be maximum at the jet center and to fall sharply away from it. Thus vibrations of the pitot tube due to impact of moving particles or a slight error in exact centering of the probe may give substantially different values. This may become more evident from the comparison of experimental axial gas velocities referred to as "at jet axis" and the theoretical axial gas velocities, as shown in Figure 13. Close to the jet entrance the experimental results are close to the theoretical values at the jet center but away from the entrance the computed axial velocities at 2.5 mm away from the axis have a far better agreement with the experimental data.

Similar inaccuracies may exist in estimation of solid velocities calculated from movies. In Figure 14 the computed axial solid velocities are compared to the data. Both theoretical and experimental solid velocities are small at the jet inlet and they rise sharply within a short acceleration zone. The computational results exactly at the jet center follow the experimental data in this zone whereas during the deceleration zone, as the solids loose their momentum, the theoretical results at 2.5 mm away from the jet center have better agreement with data.

Figure 15 shows the computed and experimental solid volume fractions along the jet axis. The lower curve in Figure 15 is the solid volume fractions exactly at the jet center. The solid line shows the computed void fraction at 5 mm. away from jet axis. The experimental data lie between the two theoretical curves. Figure 15 also shows that the axial solid volume fraction rises steadily along the bed height, without going through a minimum as was observed in the Westinghouse results. The Basov's (1969) correlation yields a jet penetration height of 196 cm for 90 m/s jet velocity. This height is much higher than the 10 cm static bed height of the Donsi et al.'s experiment. Thus, as the absence of a minimum in axial void fraction shows, the high velocity jet penetrates the bed. In other words the experimental bed should have been spouting.

NOTATION

C_D = drag coefficient
d_p = diameter of solid particles, m
g = gravitational force per unit mass, m/s^2
$G(\epsilon)$ = modulus of elasticity, N/m^2
H_{mf} = minimum fluidization bed depth, m
P = pressure, Pa
Re_s = solid Reynolds number
T = temperature, °C
t = time, second
U_{mf} = minimum fluidization velocity, m/s
U_s = radial solid velocity, m/s
U_g = radial gas velocity, m/s
V_s = axial solid velocity, m/s
V_g = axial gas velocity, m/s
r = coordinate in radial direction, m
y = coordinate in axial direction, m

Greek Letters

β = fluid-particle friction coefficient kg/m^3·s
ϵ = gas volume fraction
ϵ_{mf} = porosity at minimum fluidization
ϕ_s = shape factor (sphericity)
τ = solids stress, N/m^2
μ_g = gas viscosity, kg/m·s
ρ_g = gas density, kg/m^3
ρ_s, ρ_g = solid and particle densities, kg/m^3

Subscripts

g = gas
s = solid
p = particle
mf = minimum fluidization

ACKNOWLEDGMENT

We would like to thank the Gas Research Institute for financial support of this work under GRI grants 5014-363-0137 and 5081-360-0475, "Fluidization Using Non-Equilibrium Thermodynamics," and the National Science Foundation under grant No. CPE 8209290.

LITERATURE CITED

Basov, V. A., V. I. Markhevka, T. K. Melik-Akhnazarov, and I. Orochko, "Investigation of the Structure of a Nonuniform Fluidized Bed," *J. Fluid Mech.*, **9**, No. 2, p. 263 (1969).

Davidson, J. F., "Symposium on Fluidization-Discussion," *Trans. Instn. Chem. Engrs.*, **39**, p. 230 (1961).

Davidson, J. F., and D. Harrison, "Fluidized Particles," Cambridge University Press (1963).

Donsi, G. M., L. Massimilla, and L. Colantuoni, "The Dispersion of Axi-Symetric Jets in Fluidized Beds," *Fluidization*, Eds., J. R. Grace and J. M. Matsen, p. 297, Plenum Press (1980).

Ettehadieh, B., "Hydrodynamic Analysis of Gas-Solid Fluidized Beds," Ph.D. Thesis, Illinois Institute of Technology (May, 1982).

Gidaspow, D., B. Ettehadieh, and R. W. Lyczkowski, "Computer Modeling of Fluidization of Sand in a Two Dimensional Bed with a Jet," AIChE 74th Annual Meeting, New Orleans (Nov. 8–12, 1981a).

Gidaspow, D., B. Ettehadieh, C. Lin, and R. W. Lyczkowski, "Theoretical and Experimental Hydrodynamics of a Jet in a Fluidized Bed of Particles," *Proc. Int. Symp. on Powder Technology*, Kyoto, Japan, p. 672 (1981b).

Gidaspow, D., Y. C. Seo, and Ettehadieh, "Hydrodynamics of Fluidization; Experimental and Theoretical Bubble Sizes in a Two Dimensional Bed with a Jet," *Chem. Eng. Commun.* **22**, p. 253 (1983a).

Gidaspow, D., C. Lin, and Y. C. Seo, "Fluidization in Two-Dimensional Beds with a Jet. 1. Experimental Porosity Distributions," *Indust. Eng. Chem. Fund.* **22**, p. 187 (1983b).

Fanucci, J. B., N. Ness, and R. H. Yen, "On the Formation of Bubbles in Gas-Particulate Fluidized Beds," *J. Fluid Mech.*, **94**, Part 2, p. 353 (1979).

Harlow, F. H., and A. Amsden, "A Numerical Fluid Dynamic Calculation for all Flow Speeds," *J. of Comput. Phys.*, **8**, p. 197 (1971).

Jackson, R., "The Mechanics of Fluidized Bed," *Trans. Inst. Chem. Engrs.*, **41**, p. 13 (1963a).

Jackson, R., "The Mechanics of Fluidized Bed," *Trans. Inst. Chem. Engrs.*, **41**, p. 22 (1963b).

Jackson, R., "Fluid Mechanical Theory," *Fluidization*, Eds., J. F. Davidson and D. Harrison, p. 63, Academic Press (1971).

Keairns, D. L., "Fluidization Large Facilities and Scale up: Strategy, Limitations, Needs," *Proc. Nat. Sci. Foundation Workshop on Fluidization and Fluid-Particle Systems-Research Needs and Priorities*, Troy, NY (Oct. 17–19, 1979).

Kos, P., "Gravity Thickening of Water Treatment Plant Sludges," *J. AWWA*, p. 272 (1977).

Lyczkowski, R. W., D. Gidaspow, and C. W. Solbrig, "Multiphase Flow Models for Nuclear, Fossil and Biomass Energy Production," *Advances in Transport Processes*," **II**, p. 198, Ed., A. S. Mujumdar, Wiley-Eastern Publisher (1982).

Lyczkowski, R. W., D. Gidaspow, C. W. Solbrig, and E. C. Hughes, "Characteristics and Stability Analyses of Transient One-Dimensional Two-Phase Flow Equations and Their Finite Difference Approximations," *Nucl. Sci. and Eng.*, **66**, p. 378 (1978).

Pritchett, J. W., H. B. Levine, T. R. Blake, and S. K. Garg, "A Numerical Model of Gas Fluidized Beds," *AIChE Symp. Ser.*, **176**, p. 134 (1978).

Richardson, J. F., and W. N. Zaki, "Sedimentation and Fluidization: Part I," *Trans. Inst. Chem. Eng.*, **32**, p. 35 (1954).

Rietma, K., and S. M. P. Mutsers, "The Effect of Interparticle Forces on Expansion of a Homogeneous Gas-fluidized Bed," *Proc. Int. Symp. on Fluidization*, Toulouse, France, p. 32 (1973).

Rivard, W. C., and M. D. Torrey, "K-FIX: A Computer Program for Transient Two Dimensional, Two Fluid Flow," Los Alamos, LA-NUREG-6623 (1977).

Rowe, P. N., "Drag Forces in a Hydraulic Model of a Fluidized Bed," *Trans. Inst. Chem. Engrs.*, **39**, p. 175 (1961).

Scharff, M. F., et al., "Simulation of Cold Flow in Agglomerating Reactors," JAYCORE 510-80-006/2112 (July, 1980).

Scharff, et al., "Computer Modeling of Mixing and Agglomeration in Coal Conversion Reactors," **I&II**, DOE/ET/10329/1211, JAYCOR (Feb., 1982).

Schneyer, G. P., E. W. Peterson, P. J. Chen, D. H. Brownell, and T. R. Blake, "Computer Modeling of Coal Gasification Reactors," Final Report to DOE, DOE/ET/10247, Systems, Science, Software (April, 1981).

Wen, C. Y., and Y. H. Yu, "Mechanics of Fluidization," *Chem. Eng. Prog. Symp. Ser.*, **62**, p. 100 (1966).

Yang, W. C., and D. L. Keairns, "Momentum Dissipation of and Gas Entrainment into a Gas Solid Two-Phase Jet in a Fluidized Bed," *Fluidization*, Eds., J. R. Grace and J. M. Matsen, p. 305, Plenum Press, (1980).

Yang, W. C., and D. L. Keairns, "Solid Entrainment Rate into Gas and Gas-Solid Two-Phase Jets in a Fluidized Bed," 2nd World Cong. of Chem. Engineering, Montreal, Canada (Oct. 4–9, 1981).

Manuscript received August 2, 1982; revision received June 2, and accepted July 11, 1983.